EVLA Memo – 101
Multi Frequency Synthesis Imaging for the EVLA : An initial investigation

Urvashi R.V.,* T.J.Cornwell†, S.T.Myers‡

April 12,2006

Abstract

This document presents an analysis and comparison of existing multi frequency synthesis algorithms along with some hybrids, from the point of view of (E)VLA wide-band imaging requirements of $\sim 1\mu$Jy rms noise and $> 10^6$ dynamic range from an 8 hour observation over a bandwidth of 1GHz at L Band. Tests on simulated wide-band data with power law (and non power-law) spectra show the following. (i) Single channel deconvolution techniques are inadequate due to the limiting single channel sensitivity and the varying spatial resolution across channels. (ii) Bandwidth synthesis along with double deconvolution techniques that model the spectral variation as a power law work well for sources with pure power law spectra. For non power-law spectra, especially with large scale weak emission, inaccuracies in the estimation of the actual spectral signature of the sources lead to deconvolution artifacts at the 10μJy level. (iii) Hybrid techniques that combine single channel imaging and bandwidth synthesis using a power law model for spectral flux variation, work well when only bright and compact sources have significant spectral flux variation. Therefore, alternate algorithms (or variants) must be devised to extend the modeling of the spectral flux variation beyond that of a pure power law and simultaneously account for the accurate deconvolution of extended emission.

*National Radio Astronomy Observatory/New Mexico Tech, Socorro,NM 87801, USA.
email:*rurvashi@nrao.edu*

†Australia Telescope National Facility, PO Box 76, Epping, NSW 2121,Australia.
email:*tim.cornwell@csiro.au*

‡National Radio Astronomy Observatory, Socorro,NM 87801, USA.
email:*smyers@nrao.edu*

1 Introduction

Multi frequency synthesis (MFS) imaging in radio interferometry, involves gridding visibilities from different frequency channels separately to eliminate bandwidth smearing, and augmenting the deconvolution process to take into account flux variations across the observing band. The goal of any MFS algorithm is to produce a high dynamic range continuum image with minimal deconvolution errors due to spectral flux variation, while using the entire data set for increased sensitivity.

MFS imaging algorithms have so far been designed primarily from the point of view of enhanced UV coverage provided by multi channel data from relatively sparse arrays. These algorithms are reported to produce images with dynamic ranges of about 1000 to 1 and negligible deconvolution errors (within the rms noise) up to bandwidths of 25%. The Conway/Sault algorithm is currently the most advanced in terms of accounting for spectral flux variation while deconvolution, but it assumes a relative power law spectrum between image pixels which translates into the assumption of a constant spectral index across the band.

The planned EVLA bandwidths (50%) with 16384+ observing channels, are much larger than before, and have been chosen to allow the production of wide-band continuum images with increased sensitivity ($\sim 1\mu Jy$), and spatial dynamic ranges of $> 10^6$. Over these large bandwidths, the assumption of a pure power-law spectrum often breaks, and it is not clear how well the existing algorithms will perform in terms of achievable dynamic ranges and deconvolution errors due to approximately estimated spectral flux variation.

This document presents an analysis and comparison of some existing algorithms, from the point of view of wide-band imaging requirements of $\sim 1\mu$Jy rms noise from an 8 hour (E)VLA observation over a 1GHz band at L Band. Some hybrid techniques are also presented along with a suggested extension of the Conway/Sault algorithm to include component based imaging via multi-scale deconvolution. All the analysis in this report is based on data simulated in AIPS++, and algorithms implemented in AIPS++ and Miriad.

2 Sensitivity Calculations

EVLA system specifications for an 8 hour VLA C array observation with a 1GHz bandwidth at L Band give Stokes I image sensitivities calculated as follows.

The sensitivity (lowest detectable flux above the noise) for the output from a single baseline (or, the noise per visibility value) is given by

$$\Delta V_{ij} = \frac{1}{\eta_s} \frac{SEFD}{\sqrt{2\Delta\nu\tau_{acc}}} \tag{1}$$

where $SEFD = 10^{23} T_{sys}/K \ Jy$ and $K = \eta_a A/2k_B$. τ_{acc} is the per visibility

integration time in *seconds*, $\Delta\nu$ is the channel bandwidth in $Hertz$, A is the collecting area of an antenna in cm^2, η_a is the antenna efficiency, η_s is the system efficiency and T_{sys} is the antenna system temperature in K.

The image sensitivity for a single channel stokes I image (using RR and LL data) is given as

$$\Delta I_m = \frac{1}{\sqrt{2}\eta_s}\frac{SEFD}{\sqrt{N(N-1)\Delta\nu\tau_{int}}} \quad (2)$$

where τ_{int} is the total integration time in *seconds*. The factor of $\sqrt{2}$ in the denominator is for the two independant data channels (RR and LL). The image sensitivity for a multi-frequency image over N_{ch} channels is given as $\Delta I_m/\sqrt{N_{ch}}$.

In terms of eqn 1, this is equal to the numerical estimate based on the number of data points as given by

$$\Delta I_m = \frac{\Delta V_{ij}}{\sqrt{\frac{N(N-1)}{2}N_{ch}N_tN_{pol}}} \quad (3)$$

where $N_t = \tau_{int}/\tau_{acc}$ is the number of timesteps and $N_{pol} = 2$ for a stokes I image that uses the RR and LL polarizations.

Below are a set of observation parameters and corresponding image sensitivities.

$T_{sys} = 35K$,$\eta_a = 0.55$,$\eta_s = 0.78$,$N = 27$,$A = \pi(1250^2)cm^2$,$\tau_{int} = 8hr$, $\tau_{acc} = 300sec$,$\Delta\nu = 10MHz$,$N_{ch} = 128$ and $N_{pol} = 2$.

```
SEFD :  357.803  Jy
Total effective bandwidth :  1280  MHz
Noise per visibility :  5.92e-03  Jy
Image Sensitivity :  2.01e-06  Jy
```

With $N_{ch} = 32$ and a total bandwidth of $320MHz$ spread over $1280MHz$, the sensitivity is multiplied by $\sqrt{4}$ to correct for the smaller number of channels, to give 4.03e-06 Jy.

3 MFS Simulations and Results

3.1 Simulation Parameters

Point source data was simulated with five point sources with peak flux levels of 100mJy, 10mJy, 1mJy, 100μJy, 10μJy. The single channel noise was comparable to the flux of the weakest source. In simulations with non-zero spectral index, only the 10mJy source had a non-flat spectrum over the observing bandwidth of 1.2GHz.

Extended emission data was simulated with five components as per the flux and spectral characteristics of a typical core-jet-hotspot. The brightest component (100mJy) had a

Table 1: Data Simulation Parameters

Array	VLA C array
Observing Band	LBand (1420MHz)
Total Bandwidth	320MHz (spread over 1280MHz)
Delta ν	40MHz
Frequency Resolution	10MHz
Frequency range	785MHz to 1985MHz
Reference Frequency	1420MHz
Number of channels	32
Cell size	2 arcsec
Image size	1024x1024 pixels
Image field of view	34 arcmin
Integration timestep	300 s
Total integration time	8 hours
Number of timesteps	8*3600/300=96
Noise per visibility	1e-03 Jy
RMS noise in single channel image	1e-03/$\sqrt{351 * 1 * 96 * 2}$=3.85e-06
RMS noise in mfs image	1e-03/$\sqrt{351 * 32 * 96 * 2}$=6.8e-07
Expected Dynamic Range	0.1/6.8096e-07=1.468e+05

flat spectrum, the 10mJy hotspot had a spectral index of 0.7, and the diffuse 'jet' had flux levels between 10μJy and 100μJy with spectral index varying between 0.1 and 0.5.

Parameters used in the simulations for testing the current algorithms are as follows. They correspond to a T_{sys} of about 20K, and η_a and η_s around 0.80.

Note : Only 32 channels were used because of data processing restrictions at the time of performing these tests. Algorithms that manipulate image cubes in AIPS++ load entire cubes and thus lead to errors because of limited usable RAM and AIPS++ tiling bugs. The true VLA antenna specifications could have been used along with a larger number of channels, and larger total obsrvation time to give the same $\sim 1\mu$Jy rms noise. Increasing the number of channels and thus reducing the rms noise in the MFS

image, would clearly demonstrate the disappearance of a weak source within the single channel noise for single channel deconvolution techniques.

Computational requirements arising from the large number of channels being planned (16384+), and the potential effect this may have on the structure of the algorithms, have not yet been investigated for multi-frequency synthesis imaging.

3.2 Algorithms

Channel Averaging (AVG)	Bandwidth Synthesis (BWS)	Multi Frequency Clean (MFC)
The simple technique of deconvolving each channel separately, and computing the final value per pixel by averaging over the frequency axis.	Grid visibilities from each channel onto separate uv tracks to avoid bandwidth smearing, and perform a single deconvolution to obtain a continuum map with no spectral information retained. (AIPS++ MFS settings in `imager`)	Grid visibilities from each channel onto separate uv tracks and perform a double deconvolution to obtain a continuum map as well as an effective spectral index map (first two terms of a Taylor expansion in ν). (MIRIAD mfclean).
(+) Simple with no deconvolution errors due to spectral variation.	(+) Performs a joint deconvolution that benefits from the added sensitivity gain of using data from all channels together. Works well for flat spectrum sources.	(+) Performs a joint deconvolution across channels and also produces an effective spectral index map. Works for power law spectra with a fixed spectral index across the band.
(−) Sensitivity is limited by single channel noise. Sources that are fainter than the single channel noise will not be detected and cannot be accurately recovered after averaging. Also the relatively sparse uv coverage will produce more structural errors related to deconvolution. Resolution is limited by the largest clean beam.	(−) This algorithm assumes that all sources in the image have a flat spectrum across the frequency band. If the spectrum of a source is not flat, all visibility values after combined gridding of multi channel data do not represent the same source flux and deconvolution errors will occur. A modification to scale all channels according to an average spectral index (over all sources) will reduce deconvolution errors.	(−) The current miriad implementation of MFClean fits for a log linear spectrum with a fixed effective spectral index per image pixel. Deconvolution errors result when the spectrum is not log linear (for example, a non-zero first order spectral index term, or a turnover feature). Low level extended emission is not completely deconvolved.

3.3 Results

Figures 1-7 show the reconstructed image and the corresponding residual image for each algorithm, along with a set of measures to compare the relative accuracies of the algorithms. Separate estimates for on-source and off-source regions were computed using masks created by thresholding the known true image at a 2σ level. Only the inner quarter of each image was considered for CLEANing. All results are based on automated runs of existing standard algorithms on simulated data. Carefully tuned deconvolution could in some cases result in better reconstructions.

Listed along with the results of each sample run are the following quantities.

1. Off source RMS : The achieved noise level in regions away from the true source.
2. Peak residual : The magnitude of the peak of the residual image. It represents the flux level of the minimum detectable/believable feature.
3. Dynamic Range (w.r.t. rms) : The ratio of the peak of the resonstructed image to the off-source rms. It represents the maximum dynamic range achieved in the image.
4. Dynamic Range (w.r.t. peak residual) : The ratio of the peak of the reconstructed image to the peak residual. It represents the achieved dynamic range w.r.t. believable features.
5. $\chi^2_{normalized}$ [1] (entire image) : A measure of image fidelity, computed as the normalized χ^2 between the reconstructed image and the known true image. This number represents the total power present in the difference image, in multiples of the expected thermal noise level.
6. $\chi^2_{normalized}$ (on-source) : A measure of image fidelity via normalized χ^2, computed only over on-source pixels chosen via a mask. It estimates the total power present in the difference image in regions of known non-zero flux and measures the accuracy of the on-source reconstruction, with respect to the thermal noise level.
7. $\chi^2_{normalized}$ (off-source) : A measure of image fidelity via normalized χ^2, computed over off-source pixels. Any deconvolution errors resulting in spurious features in regions of no true flux, are reflected in this estimate.

[1] $\chi^2_{normalized}$ computed as $\frac{\frac{1}{n-1}\sum_i^n (I_n^{restored} - I_n^{true})^2}{\sigma^2_{thermal}}$ is equivalent to the F-statistic used to compare sample sets of different variances (see Appendix II). The absolute error on $\chi^2_{normalized}$ is based on the number of points used in the computation, and is derived from the expression of variance of the F-statistic. Few merits of using $\chi^2_{normalized}$ to estimate image fidelity instead of the median image fidelity estimate given by $median[I_n^{restored}/(I_n^{restored} - I_n^{true})]$ are as follows. $\chi^2_{normalized}$ has an ideal value of 1.0 corresponding to a true reconstruction and this can be used as a reference value. It is a statistically sound measure that is sensitive to any non-zero mean flux in the difference image as well as to the difference between the achieved rms noise and the expected thermal noise level. Also, $\sqrt{\chi^2_{normalized}}$ represents the total deviation as a multiple of the thermal noise ($n\sigma$).

3.3.1 Point Sources

1. Figure 1 shows the results for a run with zero spectral index. The AVG restored image shows relatively broadened components due to the varying spatial resolution for each channel. The residuals show traces of all sources implying that the amplitudes and shapes of all the flux components have not been recovered well enough. On this run, deeper CLEANing was not possible on the individual channels due to the limiting single channel noise. The high on-source and off-source $\chi^2_{normalized}$ estimates reflect this.

   The MFC and BWS results show no extended deconvolution errors, and reach rms levels $1-2\sigma$, producing the expected dynamic range of 10^5 for this image. The peak flux reconstruction was accurate to approximately 1σ for both the BWS and MFC algorithms with $\chi^2_{normalized} \approx 25$. (The high on-source $\chi^2_{normalized}$ for the MFC algorithm is the result of a slight difference in the restoring beams used by AIPS++ and MIRIAD.).

2. Figure 2 shows the results for a run where one source has a spectral index of 0.5. The AVG images show no errors due to the changing spectral index of one source but have incorrect flux levels and the effect of varying spatial resolution. The image fidelity and residuals remain relatively poor.

   The BWS images show the effects of not taking into account the changing spectral index of one source. Deconvolution errors around this source arise because of the difference between the actual and assumed flux levels in each channel. A factor of 100 increase in on-source $\chi^2_{normalized}$ in comparison to that in Figure 1 reflects this.

   The MFC images show the result of fitting for a log-linear spectrum in terms of an effective spectral index parameter. There are no extended deconvolution errors down to the level of the thermal noise, and the expected maximum dynamic range of 10^5 is acheived.

3. Figure 3 shows the results for a run where one source has a spectral index that varies between 0.5 and 1.6 over the observing band. The data was simulated by adding a first order term to the spectral index $\alpha_0 + (\nu - \nu_0)\frac{d\alpha}{d\nu}$.

   The AVG images show characteristics similar to the previous runs with no discernable deconvolution errors due to inaccurately modelled spectral flux variation, but with incorrect on-source flux and sensitivity limited by the single channel noise level.

   The BWS images show significantly more deconvolution error around the source in question. This is also reflected in the reduced dynamic ranges, and higher on-source $\chi^2_{normalized}$ as compared to previous runs. The MFC images also show error, but due only to the changing α. These errors are at the 2σ level and result in higher residuals and therefore lower maximum dynamic range.

3.3.2 Point Sources : Hybrid techniques

The following techniques are based on estimating spectral index information from single channel maps. There are three sources of error in this approach. First, the single channel noise limits the sensitivity of each image in the stack and this can be improved only by deconvolving all channels together. Second, since the channel deconvolutions are independant of each other, there will be noise associated with the spectral variation across channels and this can be reduced by fitting a smooth function to the spectral variation to estimate the spectral index. Third, the resolution element varies in size across channels and can be a source of positional uncertainty in each component. This too can be improved only by deconvolving all channels together.

1. MFC+AVG (Figure 4(left))

   (a) Divide data into chunks of frequency channels.

   (b) Perform MFClean on each chunk.

   (c) Average the final maps together.

   This technique is equivalent to approximating the spectrum due to a varying spectral index by a piecewise log linear spectrum. It gives images which do not show deconvolution errors due to a non-flat spectrum, but the noise level is higher due to the individual deconvolutions having less sensitivity. This also raises the possibility that the deconvolution features are just being masked and not eliminated. Also, the full resolution of the combined psf is not obtained.

2. BWS+AVG (Figure 4(middle))

   (a) Deconvolve each channel separately and estimate the shape of the spectrum per pixel by fitting to the image cube.

   (b) Flatten out the image cube by rescaling each channel per pixel by the estimated spectrum.

   (c) Predict new flat spectrum visibilities and perform a Bandwidth Synthesis.

   (d) Expand the resulting model image into a spectral cube, and rescale each channel per pixel to reapply the estimated spectrum.

   This method does not show artifacts due to spectral variation, but the weakest source that was not detected in the single channel maps, was completely randomized out due to the application of 'noisy' scaling factors while flattening out the image cube.

3. AVG+BWS (Figure 4(right))

   (a) Deconvolve each channel separately, upto the single channel sensitivity limit.

   (b) Perform a visibility subtraction (using visibilities predicted from the model image cube) to remove the contribution of bright (spectrally varying) sources.

(c) At this stage, the peak brightness is at the level of the single channel noise limit. Perform an MFClean or bandwidth synthesis on the resulting visibilities.

Weak sources within the single channel noise will be detected during the third step of the procedure. If however the weakest sources are also spectrally varying beyond a power law, deconvolution errors will appear below the single channel noise level. However, depending on the continuum noise limit, the peak contribution from the higher order beams could now be negligible, and therefore may not need to be accounted for in the third step.

All three hybrid algorithms showed no discernable deconvolution errors resulting from incorrectly estimated spectral flux variation, but the on-source flux reconstructions were no better than the other algorithms.

3.3.3 Error Analysis

Following the discussion from section 2.3 of Conway,Cornwell,Wilkinson,1990, estimated peak values of the spectral beams can be used to define noise levels above which the contribution from any residual spectral beams becomes negligible.

For point sources, the peak values of the different spectral beams can be estimated from the peak brightness and spectral index of the source. The maximum sidelobe levels for the first two higher order beams (beyond the regular psf) can be estimated to be $I\alpha/200$ for B_1, and $I\alpha^2/2000$ for B_2.

For the simulations performed in this study, this corresponds to $\sim 20 - 80\mu Jy$ and $\sim 3 - 10\mu Jy$, for the $10mJy$ source with spectral index α varying between 0.5 and 1.6.

The simulations (Figure 3) using bandwidth synthesis assuming a flat spectrum show peak residuals at $10\mu Jy$, and considerable deconvolution errors. The MFClean algorithm which takes into account the first order beam, shows peak residuals at $\sim 8\mu Jy$, which are at the level expected for the unaccounted-for second order beam.

For the AVG+BWS hybrid, at the end of second step, the peak flux was at the single channel noise level of $\sim 4\mu Jy$, leading to a peak first order beam sidelobe at $0.14\mu Jy$. This is lower than the theoretical continuum limit of $0.7\mu Jy$, and a flat-spectrum assumption sufficed.

3.3.4 Extended Sources

Extended emission data was simulated with five components as per the spectral characteristics of a typical core-jet-hotspot. The brightest component (100mJy) had a flat spectrum, the 10mJy hotspot had a spectral index of 0.7, and the diffuse 'jet' had flux levels between 10μJy and 100μJy with spectral index varying between 0.1 and 0.5.

Figures 5, 6 and 7 show the results for runs with this extended source, for total bandwidth of 320MHz, 640MHz, and 1200MHz respectively.

The AVG image shows low level large scale deconvolution errors arising from the limiting single channel sensitivity. The BWS algorithm produced more accurate on-source flux reconstruction with no discernable large-scale deconvolution errors. It shows errors primarily due to the spectrally varying flux of one source. The MFC algorithm was able to model a power-law component of the spectrally varying source, and reach a lower residual rms, but low level large scale deconvolution errors remain at the $10\mu Jy$ level. None of the algorithms reached the expected thermal noise and dynamic range.

Comparing the results from figures 5, 6 and 7, the only noticeable trend is that large scale low level deconvolution errors decrease with larger total bandwidths (and hence more total flux variation). Note that the separation in frequency between individual channels has been scaled according to the total bandwidth.

4 Conclusions

Existing multi frequency synthesis algorithms were tested on simulated wide band data, with the goal of determining how they perform against the requirement of $O(10^6)$ dynamic range and $O(1\mu Jy)$ image sensitivity. Tests were performed on data with point sources as well as extended flux components. The results were evaluated based on achieved rms levels as compared to the theoretical expected thermal noise, achieved dynamic ranges as compared to those expected, the amount of large scale deconvolution error, and image fidelity in terms of χ^2 between the restored image and a known true image, normalized w.r.t. the expected thermal noise.

1. Single channel imaging and averaging is by itself inadequate, due to the single channel sensitivity limit and the varying spatial resolution across channels. Hybrid techniques that combine single channel imaging along with bandwidth synthesis using a power law model for spectral flux variation, are applicable only to data in which only bright sources have a power-law spectrum. Also, the reconstructed on-source flux tends to depend on the algorithm used, and low level emission with varying flux across channel (as is often the case with extended emission), is not deconvolved accurately enough.

2. Pure bandwidth synthesis assuming a flat spectrum for all sources reaches 2σ rms levels, and approximately gives the expected dynamic range. On-source flux reconstructions accurate to within the noise for flat-spectrum sources. Deconvolution artifacts however surround sources with a non flat spectrum, reducing the dynamic range w.r.t. the peak residual by an order of magnitude.

3. Bandwidth synthesis with techniques to estimate and fit for power law spectral variations via coefficients of a series expansion across frequency (Conway/Sault double deconvolution), work for sources with power law spectra. For point sources

with pure power-law spectra, the MFClean algorithm reaches 1σ rms levels and expected dynamic ranges. Point sources with non power-law spectra result in 10μJy level errors. For extended sources with large scale weak emission and non power law spectra, inaccuracies in the estimation of the spectral signature of the large scale emission leads to large-scale deconvolution artifacts at the 10μJy level. In most cases, the dynamic range w.r.t. the peak residual is an order of magnitude lower than the maximum expected dynamic range (calculated w.r.t. the off source rms).

Note that in both cases, an average spectral index across the entire image can be estimated and corrected for and if all sources have similar spectral flux variation, this could considerably reduce the deconvolution errors.

Conway/Sault double deconvolution involves the simultaneous deconvolution of the regular dirty beam as well as a spectral dirty beam corresponding to the first order term of a series expansion of the flux estimate as a function of frequency. It is currently a CLEAN based point source model deconvolution. Also, for large bandwidths, the power-law assumption is likely to break down, and the higher order terms of α need to be corrected for as well. Therefore, a scale sensitive variant of the double deconvolution algorithms along with the estimation of higher orders of the series expansion, should considerably improve the performance by reducing the error due to incorrectly estimated flux variation across the band as well as deconvolution errors in the case of extended emission. A multi scale extension to the Conway/Sault algorithm is currently being worked on.

5 References

1. J.E.Conway,T.J.Cornwell,P.N.Wilkinson, *Multi-frequency synthesis: a new technique in radio interferometry imaging*, Mon.Not.R.astr.Soc.(1990)246,490-509.

2. R.J.Sault,J.E.Conway, *Multi-Frequency Synthesis*, Synthesis Imaging in Radio Astronomy II, ASP Conference series, Vol.180,1999,419-432.

3. R.J.Sault,M.H.Wieringa, *Multi-frequency synthesis in radio interferometric imaging*, Astron.Astrophys.Suppl.Ser.,108,1994,585-594.

4. J.M.Wrobel,R.C.Walker, *Sensitivity*, Synthesis Imaging in Radio Astronomy II, ASP Conference series, Vol.180,1999,171-186.

Appendix I : Images and Statistics

Figure 1: Point Sources with spectral index $\alpha = 0.0$ (flat spectrum) : AVG,BWS,MFC (top) Restored Image (bottom) Residual Image

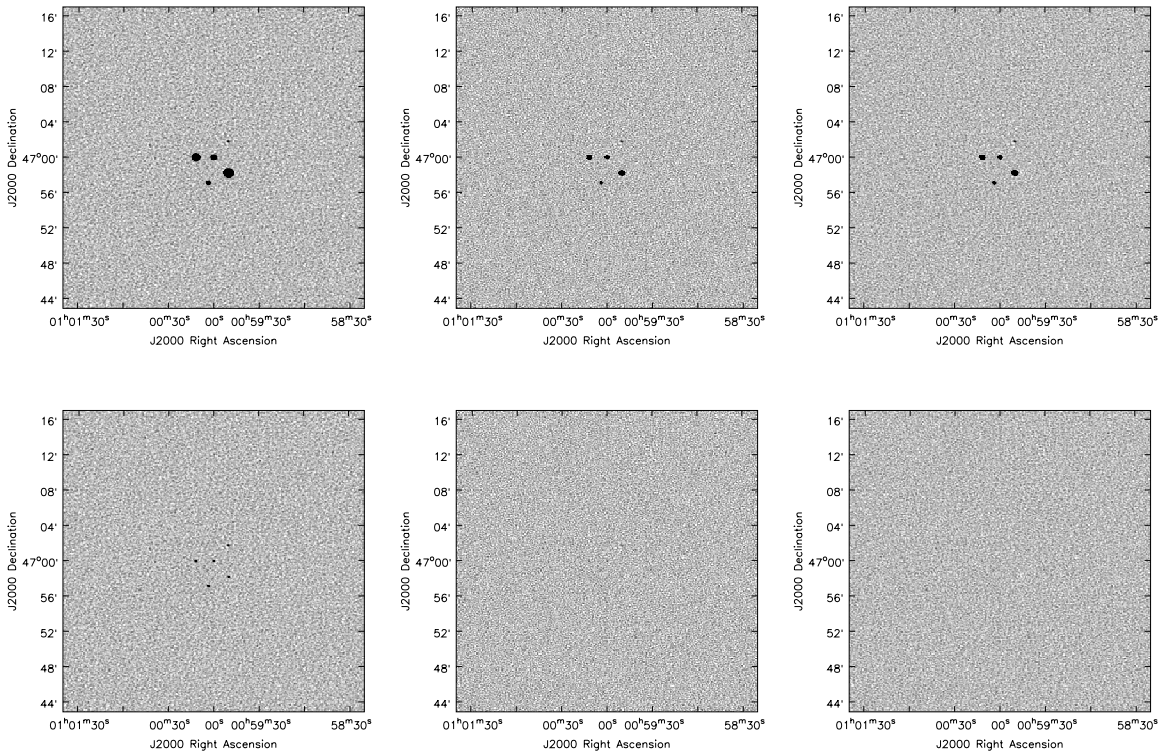

Image statistics

Flat Spectrum point sources	Off-source RMS (Jy)	Peak residual (Jy)	Dynamic Range (w.r.t. rms)	Dynamic Range (w.r.t. peak residual)
Channel Averaging (AVG)	1.008e-06	2.165e-05	9.916e+04	4.618e+03
Bandwidth Synthesis (BWS)	1.122e-06	5.66e-06	8.911e+04	1.767e+04
Sault Algorithm (MFClean)	9.369e-07	4.689e-06	1.067e+05	2.133e+04

Image fidelity in terms of χ^2 between the restored image and a known true image, normalized with respect to the expected thermal noise.

Algorithm	Entire image $\chi^2_{norm} \pm$ 0.001953	Weighted on source $\chi^2_{norm} \pm$ 0.05112	Weighted off source $\chi^2_{norm} \pm$ 0.001953
AVG	1.981e+04	2.696e+07	1.105e+02
BWS	1.041e+00	2.497e+01	1.024e+00
MFClean	3.841e+03	5.255e+06	1.124e+00

Figure 2: Point Sources with $\alpha = 0.5$ for one source (log linear spectrum) : AVG,BWS,MFC (top) Restored Image (bottom) Residual Image

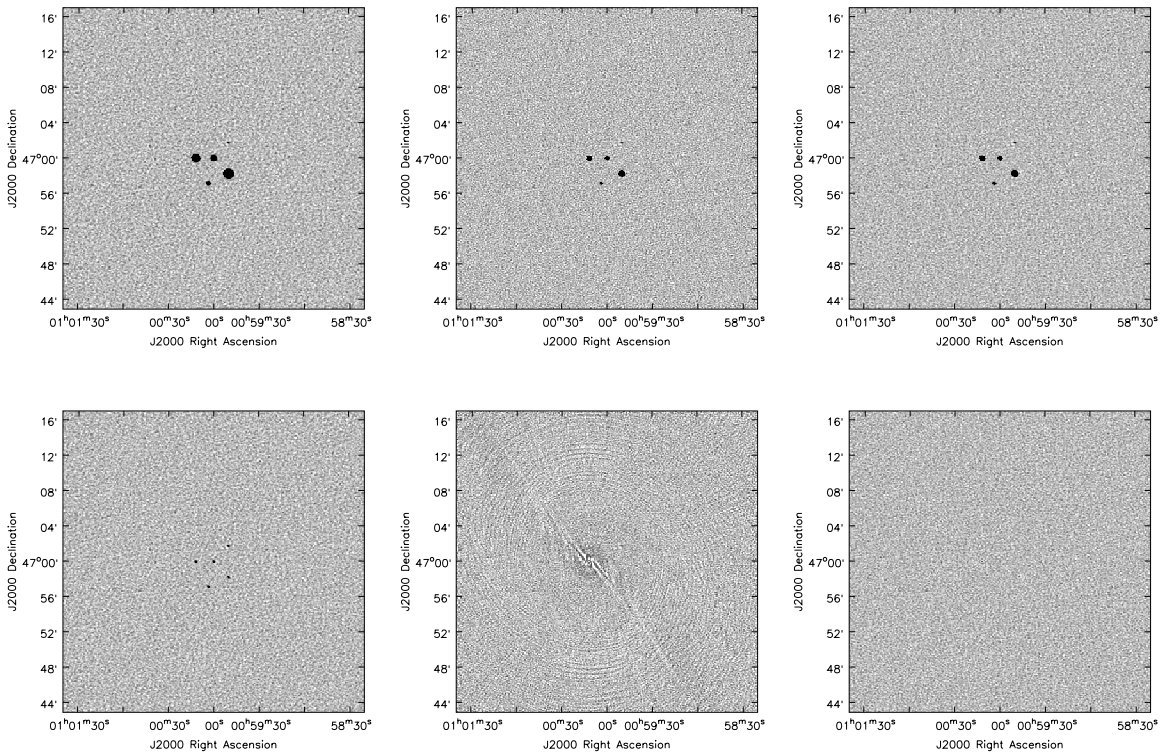

Image statistics

Point Sources with spectral index = 0.5 for one source (log linear spectrum)	Off-source RMS (Jy)	Peak residual (Jy)	Dynamic Range (w.r.t. rms)	Dynamic Range (w.r.t. peak residual)
Channel Averaging (AVG)	1.009e-06	2.163e-05	9.912e+04	4.624e+03
Bandwidth Synthesis (BWS)	1.253e-06	7.018e-06	7.978e+04	1.425e+04
Sault Algorithm (MFClean)	9.388e-07	4.507e-06	1.065e+05	2.219e+04

Image fidelity in terms of χ^2 between the restored image and a known true image, normalized with respect to the expected thermal noise.

Algorithm	Entire image $\chi^2_{norm} \pm$ 0.001953	Weighted on source $\chi^2_{norm} \pm$ 0.05139	Weighted off source $\chi^2_{norm} \pm$ 0.001953
AVG	1.977e+04	2.719e+07	1.106e+02
BWS	2.869e+00	2.428e+03	1.115e+00
MFClean	3.805e+03	5.263e+06	1.134e+00

Figure 3: Point Sources with α varying between 0.5 and 1.6 for one source : AVG,BWS,MFC (top) Restored Image (bottom) Residual Image

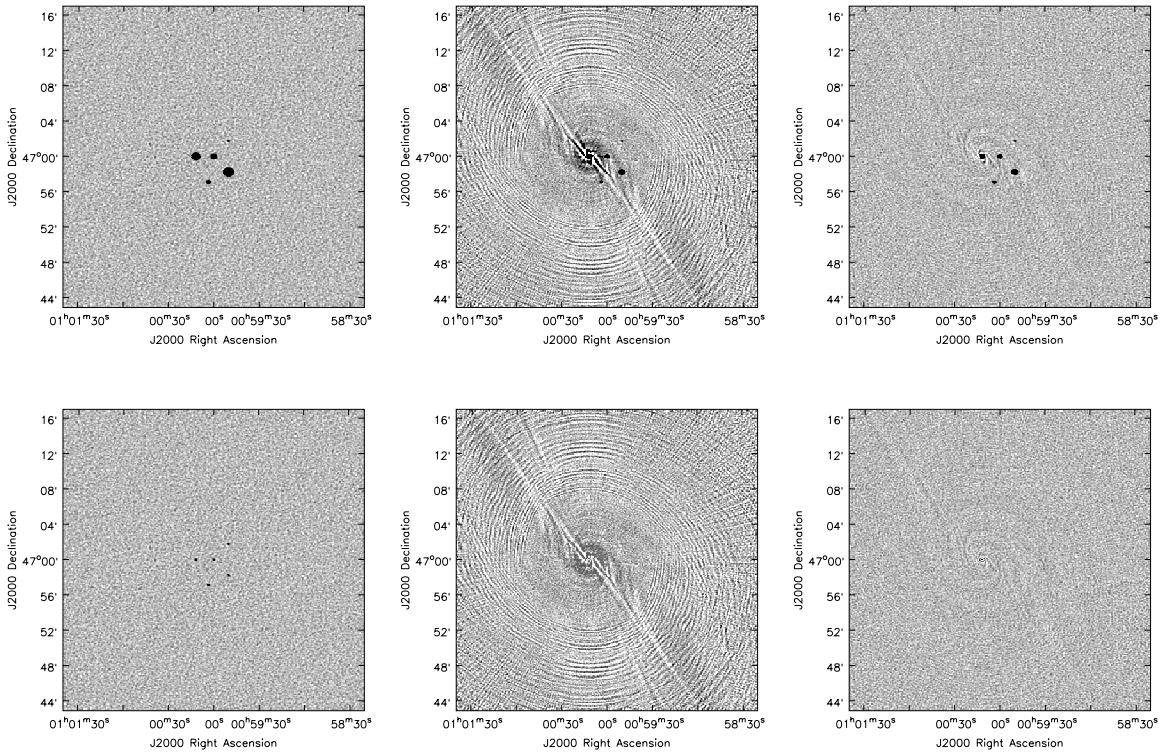

Image statistics

Point sources with spectral index varying between 0.5 and 1.6 for one source	Off-source RMS (Jy)	Peak residual (Jy)	Dynamic Range (w.r.t. rms)	Dynamic Range (w.r.t. peak residual)
Channel Averaging (AVG)	1.007e-06	2.164e-05	9.926e+04	4.621e+03
Bandwidth Synthesis (BWS)	1.849e-06	1.033e-05	5.408e+04	9.679e+03
Sault Algorithm (MFClean)	1.038e-06	9.607e-06	9.638e+04	1.041e+04

Image fidelity in terms of χ^2 between the restored image and a known true image, normalized with respect to the expected thermal noise.

Algorithm	Entire image $\chi^2_{norm}\pm$ 0.001953	Weighted on source $\chi^2_{norm}\pm$ 0.05222	Weighted off source $\chi^2_{norm}\pm$ 0.001953
AVG	1.978e+04	2.812e+07	1.126e+02
BWS	8.282e+00	9.66e+03	1.522e+00
MFClean	3.101e+03	4.427e+06	1.113e+00

Figure 4: Point Sources with α varying between 0.5 and 1.6 for one source : (top) Restored Image (bottom) Residual Image for (left) Hybrid MFC+AVG : MFC on 8 channel chunks followed by channel(chunk) averaging. (middle) AVG+BWS : Estimate spectrally varying flux from single channel maps and flatten out the visibilities before doing a BWS - high noise due to addition of sum of channel restored image, instead of working with model images. The residuals shown here are with respect to the flattened predicted visibilities and not the original data which is why they do not show the weakest source. (right) AVG+BWS with partitioning : Restored image shows only flux below the single channel noise and residual image corresponds to the complete model

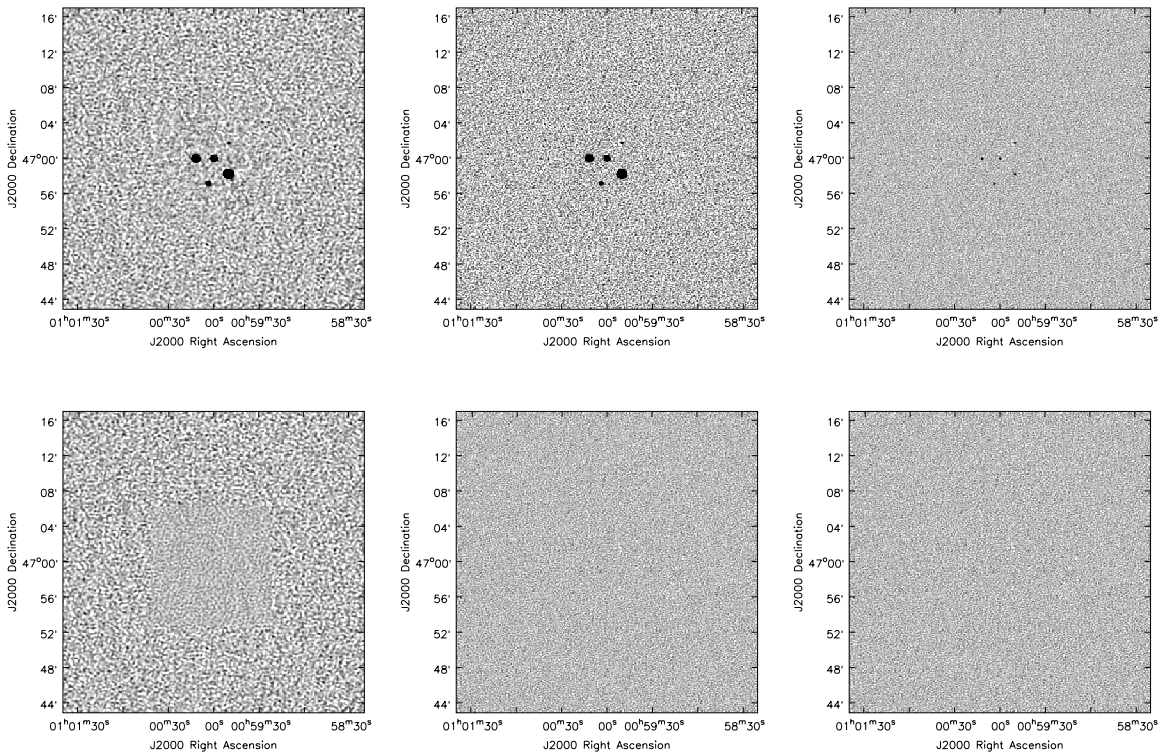

Point sources with spectral index varying between 0.5 and 1.6 for one source	Off-source RMS (Jy)	Peak residual (Jy)	Dynamic Range (w.r.t. rms)	Dynamic Range (w.r.t. peak residual)
Channel Averaging (AVG)	1.007e-06	2.164e-05	9.926e+04	4.621e+03
Bandwidth Synthesis (BWS)	1.849e-06	1.033e-05	5.408e+04	9.679e+03
Sault Algorithm (MFClean)	1.038e-06	9.607e-06	9.638e+04	1.041e+04
MFC + AVG	1.705e-06	8.607e-06	5.865e+04	1.161e+04
AVG + BWS	1.130e-06	5.733e-06	8.849e+04	1.744e+04
AVG + BWS (partitioning)	1.128e-06	5.829e-06	8.865e+04	1.715e+04

Figure 5: Extended emission with total bandwidth = 320MHz : AVG,BWS,MFC (top) Restored Image (bottom) Residual Image

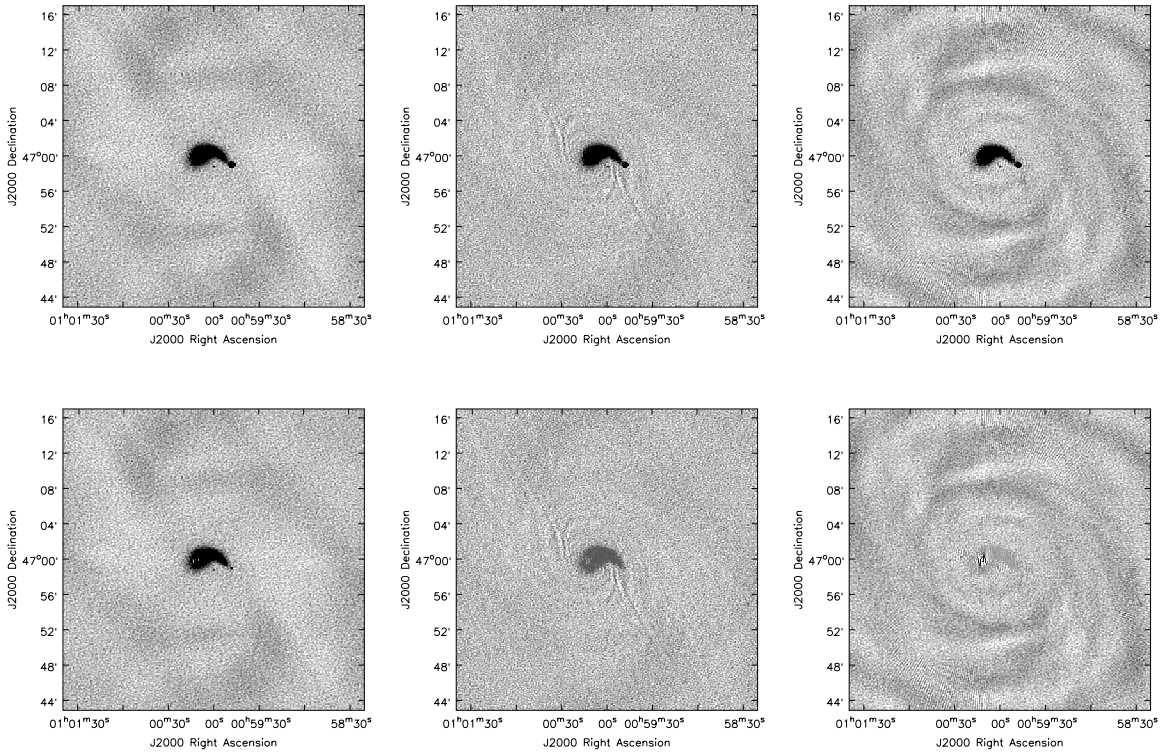

Image statistics

Algorithm	Off-source RMS (Jy)	Peak residual (Jy)	Dynamic Range (w.r.t. rms)	Dynamic Range (w.r.t. peak residual)
Channel Averaging (AVG)	1.501e-06	2.146e-05	6.662e+04	4.659e+03
Bandwidth Synthesis (BWS)	1.196e-06	5.284e-06	8.361e+04	1.892e+04
Sault Algorithm (MFClean)	1.203e-06	1.813e-05	8.313e+04	5.515e+03

Image fidelity in terms of χ^2 between the restored image and a known true image, normalized with respect to the expected thermal noise.

Algorithm	Entire image $\chi^2_{norm}\pm$ 0.001953	Weighted on source $\chi^2_{norm}\pm$ 0.02089	Weighted off source $\chi^2_{norm}\pm$ 0.001955
AVG	6.119e+03	1.394e+06	1.303e+00
BWS	1.208e+03	2.751e+05	1.099e+00
MFClean	3.756e+03	8.556e+05	1.166e+00

Figure 6: Extended emission with total bandwidth = 640MHz : AVG,BWS,MFC (top) Restored Image (bottom) Residual Image

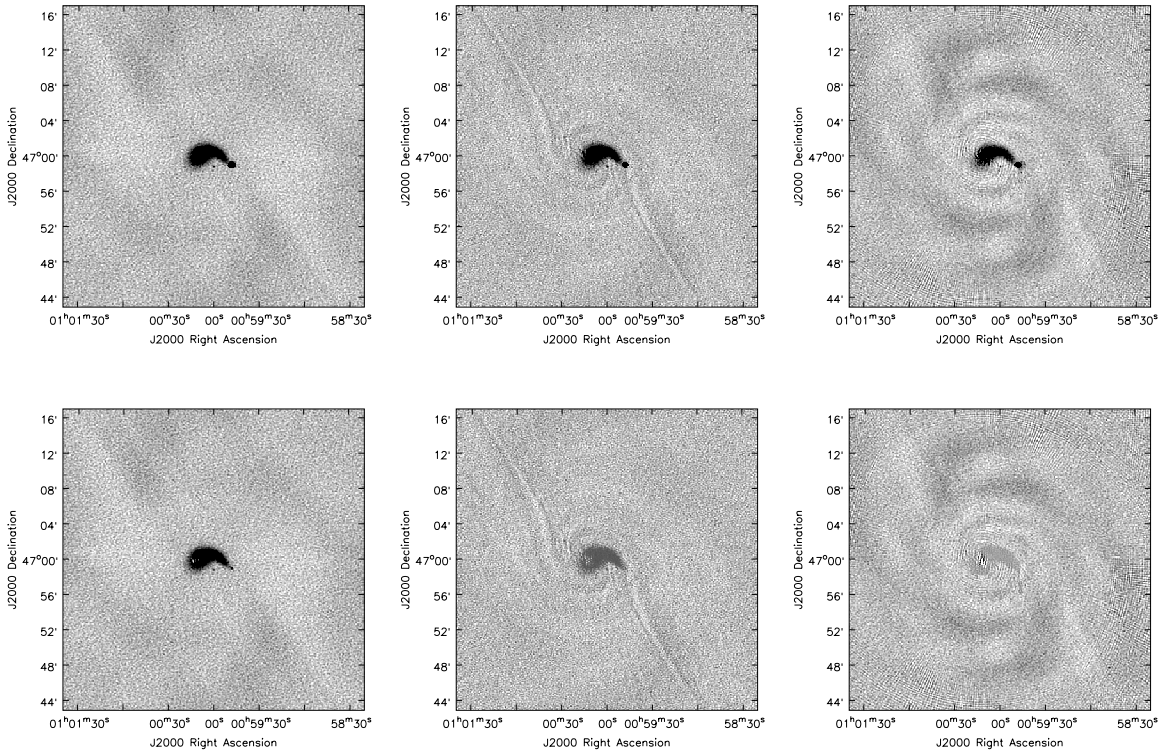

Algorithm	Off-source RMS (Jy)	Peak residual (Jy)	Dynamic Range (w.r.t. rms)	Dynamic Range (w.r.t. peak residual)
Channel Averaging (AVG)	1.445e-06	2.142e-05	6.920e+04	4.6683+03
Bandwidth Synthesis (BWS)	1.206e-06	6.041e-06	8.291e+04	1.655e+04
Sault Algorithm (MFClean)	1.233e-06	1.214e-05	8.110e+04	8.237e+03

Image fidelity in terms of χ^2 between the restored image and a known true image, normalized with respect to the expected thermal noise.

Algorithm	Entire image $\chi^2_{norm}\pm$ 0.001953	Weighted on source $\chi^2_{norm}\pm$ 0.02147	Weighted off source $\chi^2_{norm}\pm$ 0.001955
AVG	7.693e+03	1.852e+06	2.482e+00
BWS	5.112e+02	1.228e+05	1.101e+00
MFClean	2.953e+03	7.107e+05	1.137e+00

Figure 7: Extended emission with total bandwidth = 1200MHz : AVG,BWS,MFC (top) Restored Image (bottom) Residual Image

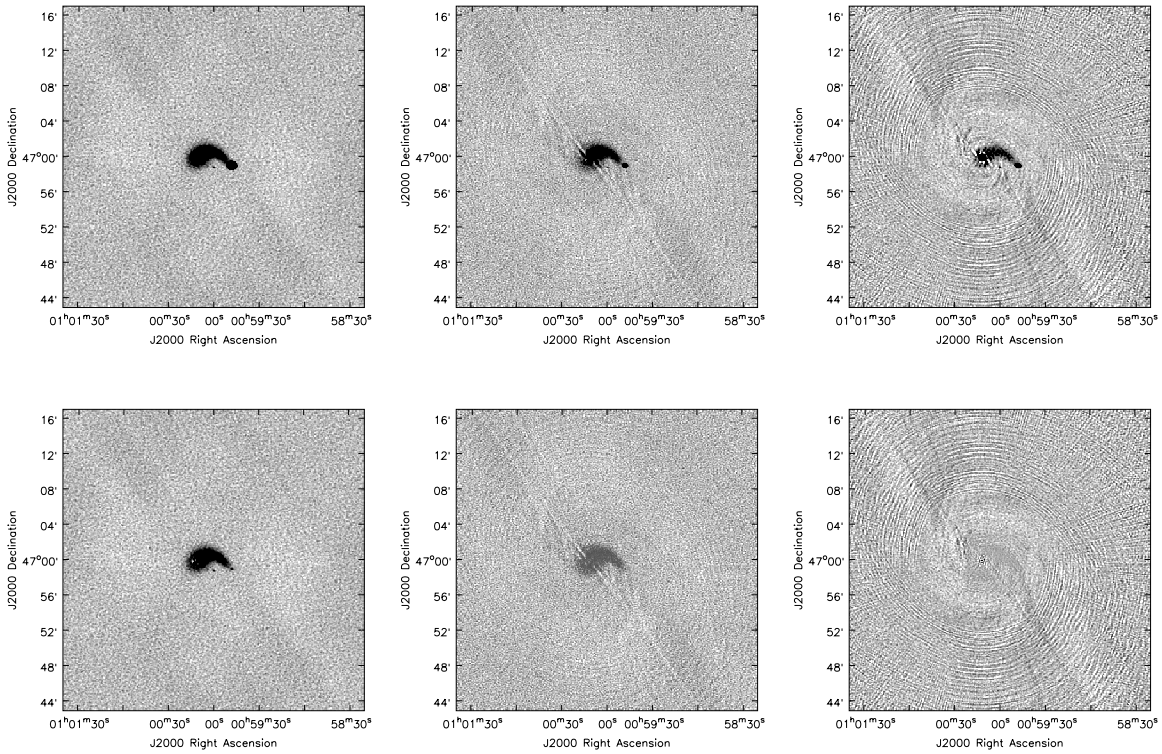

Algorithm	Off-source RMS (Jy)	Peak residual (Jy)	Dynamic Range (w.r.t. rms)	Dynamic Range (w.r.t. peak residual)
Channel Averaging (AVG)	1.398e-06	2.172e-05	7.153e+04	4.604e+03
Bandwidth Synthesis (BWS)	1.241e-06	6.016e-06	8.058e+04	1.662e+04
Sault Algorithm (MFClean)	1.562e-06	1.217e-05	6.402e+04	8.216e+03

Image fidelity in terms of χ^2 between the restored image and a known true image, normalized with respect to the expected thermal noise.

Algorithm	Entire image $\chi^2_{norm}\pm$ 0.001953	Weighted on source $\chi^2_{norm}\pm$ 0.02296	Weighted off source $\chi^2_{norm}\pm$ 0.001955
AVG	1.474e+04	4.039e+06	7.591e+01
BWS	2.292e+00	3.170e+02	1.145e+00
MFClean	1.313e+03	3.605e+05	1.092e+00

Appendix II : Image Fidelity

Let N_σ be a set of independant gaussian random samples drawn from $N(0, \sigma)$. Let S_{true} be a reference (true) image, and let $S = S_{trial} + N_\sigma$ be the sample image to be compared with the true image.

One choice of a single number to represent image fidelity is the normalized χ^2 between the S_{true} and S. This is equivalent to computing a signal to noise ratio between the total power due to signal plus noise, and the total power due only to noise. These total power estimates used in the χ^2 computation are equal to the respective autocorrelation functions, evaluated at zero lag. They are also equal to the variances, evaluated with zero mean.

The difference image D is given as

$$D = S - S_{true} = (S_{trial} - S_{true}) + N_\sigma \tag{4}$$

Let $V(D)$ denote the sample variance of D with respect to zero mean. The normalized χ^2 gives a *goodness-of-fit* estimate for the sample image S as

$$\chi^2_{normalized} = \frac{V(D)}{\sigma^2} \tag{5}$$

To get *goodness-of-fit* estimates separately for on-source and off-source regions of an image, a weight mask W comprising of zeros and ones can be used. Let n_w be the number of pixels selected by these weights. The sample variance calculated with respect to zero mean, will be given as

$$V(D) = \frac{1}{(n_w - 1)} \sum_i^n W_i D_i^2 \tag{6}$$

Here, $\chi^2_{normalized}$ is also the *F distribution statistic* used to compare between two sets of samples having different variances. One sample set is a reference noise image with true variance σ^2. The other is the difference signal D.

The merits of using Eqn 5 as an estimate of goodness of fit (and hence image fidelity) are as follows.

1. Since $V(D)$ relates to total power, the F statistic is sensitive to differences between the variance of D and that of the thermal noise (σ^2).
2. Since a zero mean is assumed in the calculation, any non-zero mean component in D will also be accounted for as it contributes to the total power.
3. The ideal case of pure thermal noise in D results in $\chi^2_{normalized}$ equal to $1.0 \pm \epsilon$.

F distribution

The *F distribution* [2] is a continuous statistical distribution which arises in the testing of whether two observed sample sets have the same variance. Let χ^2_n and χ^2_m be independent variates distributed as chi-squared with n and m degrees of freedom.

The *F statistic* is defined as the ratio of the dispersions of the two distributions

$$F_{n,m} \equiv \frac{\chi^2_n/n}{\chi^2_m/m} \tag{7}$$

The variance of the *F distribution* is given as

$$\sigma^2_F = \frac{2m^2(m+n-2)}{n(m-2)^2(m-4)} \tag{8}$$

Note that for a sample set of size n, $\chi^2_{n-1} = (n-1)\left[\frac{sample\ variance}{\sigma^2}\right]$.

Now, in our case, the reference set of size m (corresponding to all pixels in the image) is chosen to have a sample variance of σ^2.

$$\sigma^2 \equiv Sample\ Variance = \frac{1}{m-1}\sum_i^m N^2_{\sigma i} \quad \Longrightarrow \quad \frac{\chi^2_{m-1}}{(m-1)} = \frac{\sigma^2}{\sigma^2} = 1 \tag{9}$$

And for a sample set of size n_w,

$$\chi^2_{n_w-1} = (n_w-1)\frac{V(D)}{\sigma^2} \tag{10}$$

Therefore,

$$F_{n-1,m-1} = \frac{\chi^2_{n-1}/(n-1)}{\chi^2_{m-1}/(m-1)} = \frac{\chi^2_{n-1}}{(n-1)} = \frac{V(D)}{\sigma^2} = \chi^2_{normalized} \tag{11}$$

An estimate of the error on $\chi^2_{normalized}$ due to the use of different sample sizes n_w and m is given as $\sqrt{\sigma^2_F}$.

$$\Longrightarrow Goodness\ of\ Fit = \chi^2_{normalized} \pm \sqrt{\sigma^2_F} \tag{12}$$

[2] Ref : http://mathworld.wolfram.com/F-Distribution.html